International Journal of Nanomedicine

Dovepress
open access to scientific and medical research

Open Access Full Text Article

ORIGINAL RESEARCH

Down-top nanofabrication of binary $(CdO)_x(ZnO)_{1-x}$ nanoparticles and their antibacterial activity

This article was published in the following Dove Press journal:
International Journal of Nanomedicine

Number of times this article has been viewed

Naif Mohammed Al-Hada[1]
Halimah Mohamed Kamari[1]
Che Azurahanim Che Abdullah[1]
Elias Saion[1]
Abdul H Shaari[1]
Zainal Abidin Talib[1]
Khamirul Amin Matori[1,2]

[1]Department of Physics, Faculty of Science, [2]Materials Synthesis and Characterization Laboratory (MSCL), Institute of Advanced Technology (ITMA), Universiti Putra Malaysia, Serdang, Selangor, Malaysia

Abstract: In the present study, binary oxide (cadmium oxide $[CdO]_x$ (zinc oxide $[ZnO]_{1-x}$ nanoparticles (NPs) at different concentrations of precursor in calcination temperature were prepared using thermal treatment technique. Cadmium and zinc nitrates (source of cadmium and zinc) with polyvinylpyrrolidone (capping agent) have been used to prepare $(CdO)_x(ZnO)_{1-x}$ NPs samples. The sample was characterized by X-ray diffraction (XRD), scanning electron microscopy, energy-dispersive X-ray (EDX), transmission electron microscopy (TEM), and Fourier transform infrared (FTIR) spectroscopy. XRD patterns analysis revealed that NPs were formed after calcination, which showed a cubic and hexagonal crystalline structure of $(CdO)_x(ZnO)_{1-x}$ NPs. The phase analysis using EDX spectroscopy and FTIR spectroscopy confirmed the presence of Cd and Zn as the original compounds of prepared $(CdO)_x(ZnO)_{1-x}$ NP samples. The average particle size of the samples increased from 14 to 33 nm as the concentration of precursor increased from x=0.20 to x=0.80, as observed by TEM results. The surface composition and valance state of the prepared product NPs were determined by X-ray photoelectron spectroscopy (XPS) analyses. Diffuse UV–visible reflectance spectra were used to determine the optical band gap through the Kubelka–Munk equation; the energy band gap was found to decrease for CdO from 2.92 to 2.82 eV and for ZnO from 3.22 to 3.11 eV with increasing x value. Additionally, photoluminescence (PL) spectra revealed that the intensity in PL increased with an increase in particle size. In addition, the antibacterial activity of binary oxide NP was carried out in vitro against *Escherichia coli* ATCC 25922 Gram (−ve), *Salmonella choleraesuis* ATCC 10708, and *Bacillus subtilis* UPMC 1175 Gram (+ve). This study indicated that the zone of inhibition of 21 mm has good antibacterial activity toward the Gram-positive *B. subtilis* UPMC 1175.

Keywords: binary oxide $(CdO)_x(ZnO)_{1-x}$ NPs, calcination technique, antibacterial activity

Introduction

Recently, the researches related to the field of nanomaterials have been obviously growing and thus many researchers from different fields and areas have explored the unique physicochemical nanomaterials' features.[1] Therefore, several ways have allowed to create new structures, systems, nanoplatforms, or devices and can be used with many applications and fields.[2–4] One of the powerful points of biocompatible, biodegradable, and functionalized nanomaterials applications is that, more and more research works have been attracted and addressed.[5,6] The use of cubic cadmium oxide (CdO) and hexagonal zinc oxide (ZnO) semiconductors nanomaterials is one of the most important issues that has been considered with many research studies due to their unique properties individually or compositionally. CdO is a II–VI composite

Correspondence: Naif Mohammed Al-Hada; Halimah Mohamed Kamari
Department of Physics, Faculty of Science, Universiti Putra Malaysia, 43400 Serdang, Selangor, Malaysia
Tel +60 172 33 4327;
+60 123 90 6630
Email naifalhada@yahoo.com;
hmk6360@gmail.com

submit your manuscript | www.dovepress.com
Dovepress
http://dx.doi.org/10.2147/IJN.S150405

semiconductor, that is, these consist of group II and group VI elements (refer to the periodic table).[7] The distinctive nanomaterial structure's features have been explored by many applications that efficiently help produce characteristic physical and chemical properties.[8] It contains a special structure with a unique face-centered cubic crystalline as well as a metal oxide of n-type with direct and indirect energy band gaps of 2.2–2.5 eV and 1.97 eV.[9] There are a number of CdO physical applications; some examples are reviewed as follows.[10] The existence of CdO semiconductors in a form of high viability as visible light waves inside the materials is highly useful with photovoltaic applications e.g., solar cells.[11] Although clear electrodes, diodes, gas sensors, and antibacterial activity, for example, are other potential physical applications, these materials have widely been used to meet desirable requirements.[12–15] There have been several CdO nanostructures forms created at a variety of nanoscales for several purposes and applications, eg, nanoclusters,[16] nanowires and nanotubes,[17–19] nanoparticles (NPs),[20,21] nanocrystals,[22] nanorodes,[23] and many more exotic structures, eg, CdO-like nanoflower[24] and CdO nanoflake arrays,[25] among others.[26,27]

Similarly, hexagonal ZnO is a II–VI composite semiconductor made of the metallic element zinc (II) and the non-metallic element oxygen (VI).[28] Thus, many ZnO semiconductor materials have shown availability of notable characteristics that has encouraged many applications to exploit these features. This structure has been used as the standard hexagonal crystal structure and classified as an n-type semiconductor with 3.27 eV–3.50 eV direct band gaps.[29] Hence, while the unique properties of ZnO nanomaterials derived from their distinctively crystal structure and dimensions of nanosize particle, many applications and researches will take advantage of such features.[30] Antibacterial activities,[31–34] solar cells, and other optoelectronic devices have used and explored the pellucidity in the solar spectrum's observable area.[35,36] Antibacterial activity, catalysis, gas sensors, and diodes are further examples of suitable applications.[37–40] Different ZnO nanomaterial forms (such as nanorods,[41,42] nanotubes and nanowires,[43,44] nanocrystals,[45,46] nanoclusters,[47] nanofibers,[48,49] and numerous forms nanostructures) have been produced by using various methods whereas these materials revealed that different characteristics allowed for several applications to be practically produced.[50,51] As can be seen from literature, several techniques such as precipitation,[52] microwave hydrothermal,[53] sonochemical,[54,55] solvothermal,[56] chemical,[57,58] thermal treatment,[59] and sol-gel[60,61] can be used to create ZnO nanomaterials.

On the other hand, complementary characteristics could be somehow shown by the unique composition of ZnO-CdO, eg, many band gaps and sizes are created from both oxide semiconductors, with a potential probability of showing distinctive features when comparing to other singular semiconductor components.[62–64] One of the most important considerations related to the unique composition of CdO-ZnO nanocomposites is the use of ZnO-CdO with various purposes such as biocides and disinfectants. In addition, this composition has added much more stability property with longer life than organic-based materials. In addition, this composition has gained more attention in the scientific field for biological activity. CdO-ZnO nanocomposites prevent bacterial growth by cell membrane so that the damaged wall shows robust antibacterial activities on an expansive spectrum of bacteria.[65]

As found in some literature, there are several methods used to produce CdO-ZnO nanostructures, such as sol-gel method,[66–68] thermal decomposition,[69] high-pressure solution route,[70] solvothermal method,[71] solution method, and thermal evaporation.[72] But production of industrial-scale $(CdO)_x (ZnO)_{1-x}$ nanopowder by aforementioned methods has encountered restrictions due to synthetic process complexity, such as high temperature, longer reaction time, reagents toxicity, and effluent by-product manufacture. None of these methods has produced the product in binary or powder form. In addition, no reports on thermal treatment synthesis of binary $(CdO)_x (ZnO)_{1-x}$ NP have been found in literature in which an antibacterial activity study has been addressed. Thus, in order to overcome some of abovementioned drawbacks, this research has focused on the use of thermal treatment method to produce pure powder binary oxide NPs and examine the antibacterial activity. A simple thermal treatment route is used to produce no waste binary $(CdO)_x (ZnO)_{1-x}$ NP products. It is then considered as an acceptable method from an environmental perspective.[73] The novelty of this research study can be summarized as follows: the product is aimed to be produced with steady quality, low cost, more simplicity in handling, particle size control, desirable band gap, great adaptability, and powder products. These features will be attractive for various industrial-scale uses. In addition, the present method yields no toxic or environmentally harmful by-products. Furthermore, no additional chemical agents are required. This paper is dedicated to discuss a unique method that mainly and exclusively produces a binary $(CdO)_x (ZnO)_{1-x}$ nanopowder.

The prepared method has used a thermal-based treatment process to synthesize binary $(CdO)_x (ZnO)_{1-x}$ NPs and investigate the CdO and ZnO contents effect on the morphological, structural and optical properties of binary $(CdO)_x (ZnO)_{1-x}$

nanopowder. This method has used a solution with nitrate metallic ions as precursors and a PVP capping as an agent whereas a necessary calcination was done to produce pure desirable products. The morphology and crystallinity of the product were studied by different techniques. This study also has studied the antibacterial activity.

Experimental section

Materials

In this experimental work, 0.20, 0.40, 0.60, 0.80, and 1.00 mmol cadmium nitrate ($Cd(NO_3)_2 \cdot 4H_2O$ (M_W =308.46 g/mol)); 0.20, 0.40, 0.60, 0.80, and 1.00 mmol zinc nitrate ($Zn(NO_3)_2 \cdot 6H_2O$ (M_W =297.47 g/mol)); PVP ($(C_6H_9NO)_n$ (M_W =29,000 g/mol)), and deionized water as solvents were used as the starting raw materials. In this work, chemicals were purchased from Sigma-Aldrich Co., (St Louis, MO, USA); they were of standard research grade and were used without further purification.

Methodology

Firstly, the $(CdO)_x (ZnO)_{1-x}$ NP product was prepared by dissolving 4 g of PVP in 100 mL of deionized water, followed by vigorous stirring for 2 h at 70°C. Then, 0.00, 0.20, 0.40, 0.60, 0.80, and 1.00 mmol of cadmium nitrate were dissolved subsequently. Next, to form a homogeneous solution, 1.00, 0.80, 0.60, 0.40, 0.20, and 0.00 mmol of zinc nitrate were added and mixed thoroughly. After that, the mixed solution was poured into a petri dish and dried in an oven for 24 h at 80°C. The resulting solid was finally crushed for 30 min in a mortar in order to construct a powder. The obtained powder was subjected to calcination temperature of 600°C in a box furnace for 90 min. The as-synthesized and calcined samples of binary oxide NPs were ready for characterization.

Characterization

To investigate products' morphological, structural, and optical properties, powder X-ray diffraction (XRD) patterns were used; observed measurements were then recorded on an X-ray diffractometer (X'Pert Pro, PANalytical, Almelo, the Netherlands) using Cu Kα (λ=1.54187 Å) radiation at 40 kV and 30 mA. Fourier transform infrared (FTIR) spectroscopy (1650; PerkinElmer Inc., Waltham, MA, USA) measurements were made in range of 280–4,000 cm^{-1}, and transmission electron microscopy (TEM) (2010F UHR; JEOL, Tokyo, Japan) images were obtained at an accelerating voltage of 200 kV. Energy-dispersive X-ray (EDX) spectroscopy measurement was done using an EDX spectrometer (7353; Oxford Instruments, Abingdon, UK). X-ray photoelectron spectroscopy (XPS) (ULVAC-PHI Quantera II (ULVAC-PHI, Invc)) was performed utilizing monochromatic Al-K_α ($h\nu$ = 1486.6 eV); operated at 25.6 W (beam diameter of 100 μm) for the X-ray source. Wide-scan analysis was performed using a pass energy of 280 eV with 1 eV per step. Narrow scan (chemical states analysis) was performed using a pass energy of 112 eV with 0.1 eV per step. Prior to deconvolution, charge correction was performed at C 1s by setting binding energies of C-C and C-H to 284.8 eV. A UV–visible (vis) spectrophotometer (Shimadzu model UV-3600) was used in order to evaluate the optical properties of the samples at room temperature in the wavelength range between 200 and 800 nm. A PerkinElmer spectrofluorometer LS-55 equipped with a xenon lamp and room temperature conditions was used to measure photoluminescence (PL). The antibacterial activity of binary oxide NPs was investigated against bacteria on an agar plate.

Evaluation of antibacterial activity

In order to detect antibiotic proficiency of the CdO, ZnO, and CdO-ZnO NPs against bacterial infections, an antimicrobial test was performed. An investigation test was done for the samples of the in vitro antibacterial activity using a disc diffusion method. Hence, this type of investigation led to comparison of the response (sensitivity/resistance) of the microorganism with antimicrobial compounds. In addition, an activity investigation against *Escherichia coli* ATCC 25922 Gram, *Salmonella choleraesuis* ATCC 10708, and *Bacillus subtilis* UPMC 1175 Gram (+ve) was carried out for the prepared NPs. A paper disc (with a diameter equal to 6 mm) was absorbed in a suspension containing 100 mg of each NP in 10 mL deionized water. After that, a dry process was used on the paper disc and was left in an incubator. Finally, a number of papers were then placed onto plates to allow microbes to grow. The microbe culture was standardized to the 0.5 McFarland standard, approximately 10^8 cells. The plates were inverted at 30°C–37°C and also incubated for sufficient bacteria growth for a period of 2 days approximately. Subsequently, each plate was evaluated and the inhibition zone diameters were measured to the nearest millimeter after the incubation process was completed. Every test related to the evaluation process was done in triplicates and the result reported in average. Mueller Hinton agar media was used as nutrient. Streptomycin (100 mg/mL) standard and distilled water were used for each bacterium as a positive control and as a negative control, respectively. Additionally, the antibacterial test for bulk CdO, ZnO, and CdO-ZnO was compared with prepared NPs.

Results and discussions

Mechanism of NPs

Figure 1 illustrates the behavior and mechanism of development of NPs during calcining. The primary purpose of PVP was to stabilize the complex metallic salts generated. Frequently, this was attained by side steric and electrostatic stabilization of the amide groups attached to the pyrrolidone rings and the methylene groups. As the mixing solution process progressed, metallic ions become suppressed once more and trapped by the amine groups via ionic-dipole generated within polymeric chains. Then, during the drying stage, the metallic cations became stationary within the polymer cavity due to loss of H_2O. During the subsequent calcining stage, other gases evolved, eg, N_2, NO, CO, or CO_2, as organic materials decomposed. In addition, during the calcining stage, PVP influenced the generation of metal oxide NP nuclei. So, without the presence of PVP, the Ostwald ripening process would progress, increasing NP size with increased surface energy levels. However, the presence of PVP led to deactivation of the steric hindrance affecting the conglomeration of NPs.[74,75] Therefore, amendment with PVP causes a decrease in NP grain size by restricting and countering breakdown of metal ions on NP surfaces.[76–78]

XRD analysis

The XRD pattern revealing $(CdO)_x$ $(ZnO)_{1-x}$ nanoparticles formation following calcining at 600°C for 3 h is depicted in Figure 2. Diffraction peaks of ZnO and CdO NPs are marked with star and sharp, respectively, as shown in Figure 2A–D. These peaks of CdO at 2θ=33.06°, 38.340°, 55.33°, and 69.29° having relations to (111), (200), (220), and (222) planes, respectively, are clearly observed. Additionally, ZnO at 2θ=31.77°, 34.46°, 36.25°, 56.58°, 62.89°, 65.92°, and 67.93° relate to (100), (002), (101), (110), (103), (200), and (112) planes, respectively. As for the hexagonal and cubic phases of ZnO (lattice constants are a=0.325 nm; c=0.521 nm) and CdO (a=0.469 nm) NPs, these reflections are somehow assigned to the standard powder pattern. The (h k l) values are compatible with the standard card of ZnO (JCPDS file no: 36-1451) and with the standard card of CdO (JCPDS file no: 05-0640). The observed diffraction pattern is compatible with the other reported ZnCdO nanomaterial.[69,74,79,80] The synthesized binary of $(CdO)_X$ $(ZnO)_{1-X}$ NPs exhibited a mixture of cubic phase of CdO NPs and hexagonal ZnO NPs, and no other impurity peak was detected in XRD pattern of the samples. The crystal size (D) of the NPs produced can be determined following Scherrer's formula:

$$D = 0.9\lambda/\beta\cos\theta,$$

where λ is the wavelength of X-rays employed (1.5406Å), β is the full width at half maximum, and θ is the angle of diffraction. It can therefore be seen that the crystallite size has increased from 14 to 32 nm as a consequence of x values increasing to 1.00 mmol cadmium nitrate. The results demonstrate increasing x value results in sharper and narrower diffraction peaks, with increased intensity as depicted in Figure 2C, D and F. Thus, the increment in the nuclei particle size with respect to crystalline volume ratio increment has enhanced crystallinity.

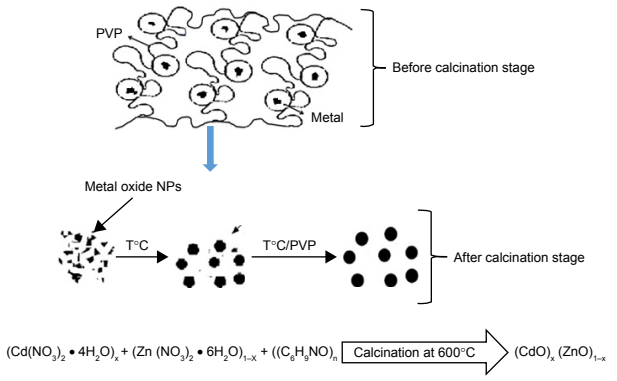

Figure 1 The proposed nanoparticle growth mechanism.
Note: Blue arrow shows metal oxide NPs after calcination.
Abbreviation: NP, nanoparticle.

SEM analysis

Scanning electron microscopy (SEM) in the range 0.00–1.00 mmol was used in order to examine the surface morphology of binary oxide NPs. Micrographs of $(CdO)_x$ $(ZnO)_{1-x}$ NPs, at six concentrations, are presented in Figure 3. The CdO and ZnO compounds appear as porous and grain shaped, respectively. Similar results were obtained within the research works reviewed by Karami et al[81] and Raja et al.[82] At high x value, as shown in Figure 3A and B. CdO has a dark color and is nearly porous with regularities, whereas the ZnO looks white and semispherical in shape. In Figure 3B–D, CdO seems as a plate form with porous shape due to tendency increment in its grains to merge, disintegrate, and overlap with x value decrement; in the ZnO image, the decrement in x is easily noticeable to produce a ZnO dispersal increment throughout the matrix due to the disintegration impact.

EDX spectrum analysis

The elemental compositions of $(CdO)_x$ $(ZnO)_{1-x}$ NPs at varying precursor concentrations following thermal treatment technique were assessed by EDX spectroscopy. The EDX spectrum derived from $(CdO)_x$ $(ZnO)_{1-x}$ NPs following

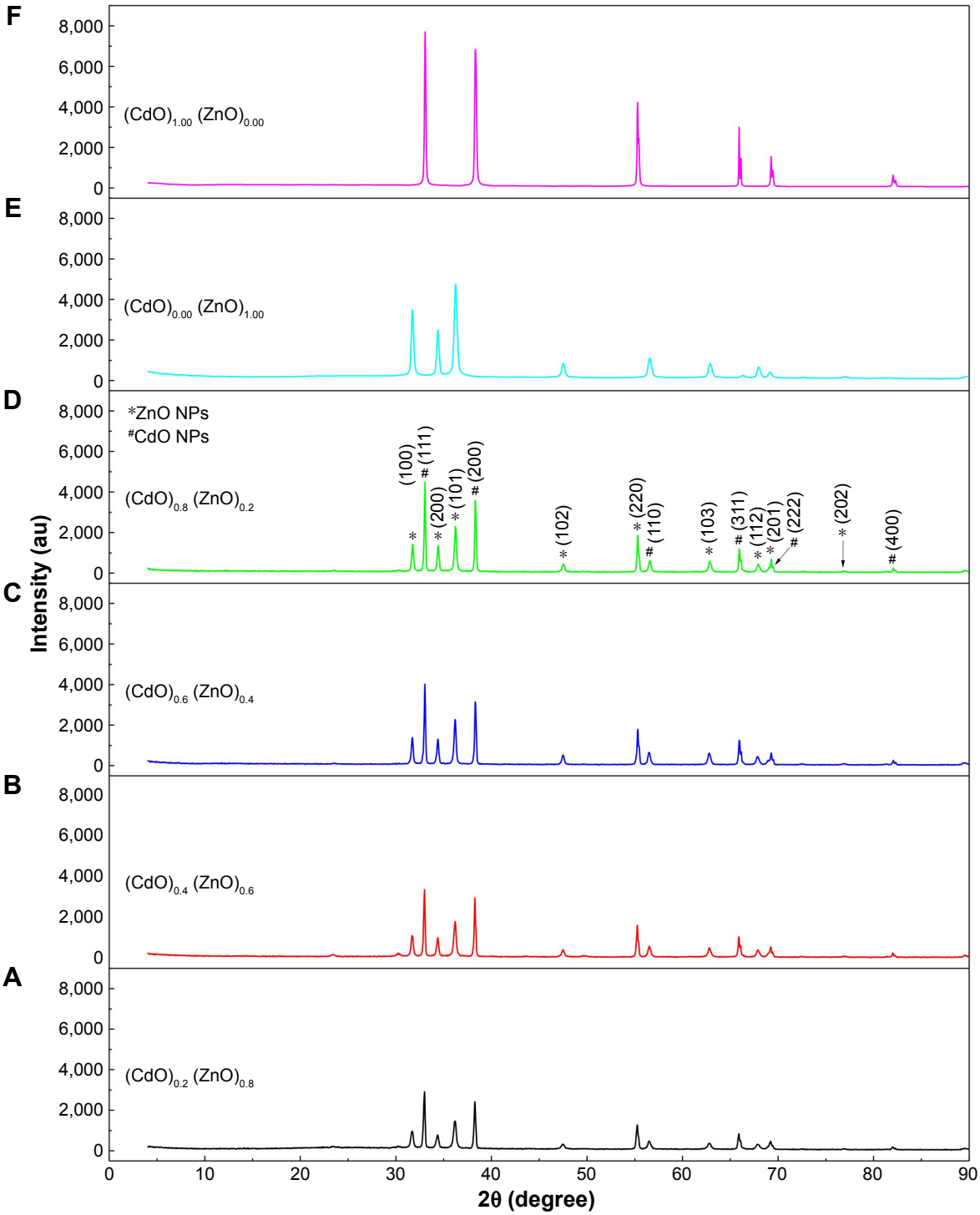

Figure 2 XRD patterns of (**A**) $(CdO)_{0.20}$ $(ZnO)_{0.80}$, (**B**) $(CdO)_{0.40}$ $(ZnO)_{0.60}$, (**C**) $(CdO)_{0.60}$ $(ZnO)_{0.40}$, (**D**) $(CdO)_{0.80}$ $(ZnO)_{0.200}$, (**E**) $(CdO)_{0.00}$ $(ZnO)_{1.00}$, and (**F**) $(CdO)_{1.00}$ $(ZnO)_{0.00}$ nanoparticles calcined at 600°C.
Note: *ZnO NPs; #CdO NPs.
Abbreviations: XRD, X-ray diffraction; CdO, cadmium oxide; ZnO, zinc oxide.

calcination at 600°C is depicted in Figure 4. These spectra reveal that the Zn:O and Cd:O elements are obviously present as the respective peaks. The atomic percentages of Zn:O and Cd:O are detailed in Table 1. This shows that the final product comprises pure binary oxide NPs. The atomic percentage of Zn:O and Cd:O appears equivalent in the final product.

TEM analysis

Characterization of the NP microstructure was determined by TEM assessment. Typically, generated samples exhibit homogeneous morphology, as illustrated in Figure 5A–D depicting TEM images of $(CdO)_x$ $(ZnO)_{1-x}$ NPs calcined at 600°C. TEM analysis corroborates the uniform spherical

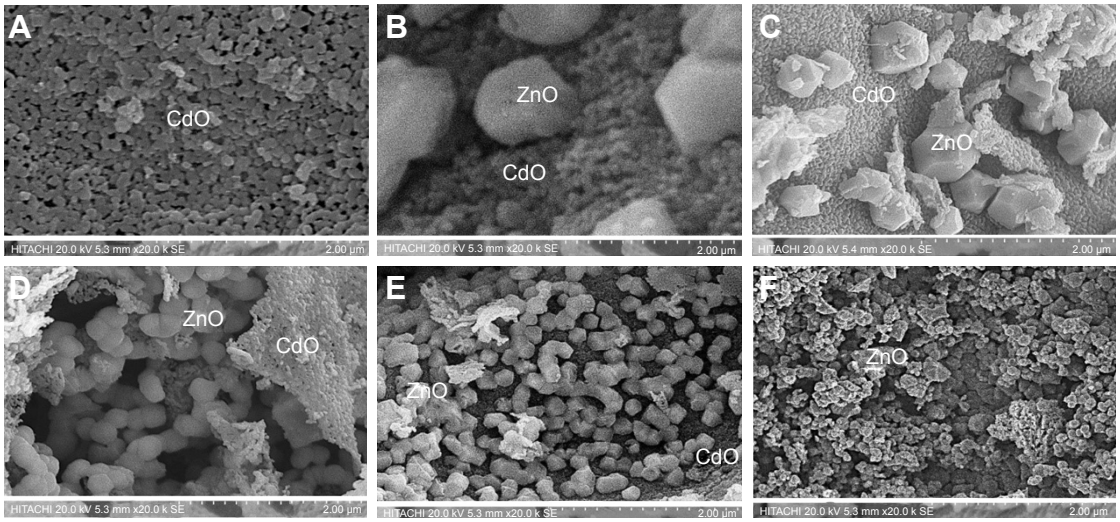

Figure 3 SEM images of (**A**) $(CdO)_{1.00}$ $(ZnO)_{0.00}$, (**B**) $(CdO)_{0.80}$ $(ZnO)_{0.20}$, (**C**) $(CdO)_{0.60}$ $(ZnO)_{0.40}$, (**D**) $(CdO)_{0.40}$ $(ZnO)_{0.60}$, (**E**) $(CdO)_{0.20}$ $(ZnO)_{0.80}$, and (**F**) $(CdO)_{0.00}$ $(ZnO)_{1.00}$ nanoparticles calcined at 600°C.
Abbreviations: SEM, scanning electron microscopy; CdO, cadmium oxide; ZnO, zinc oxide.

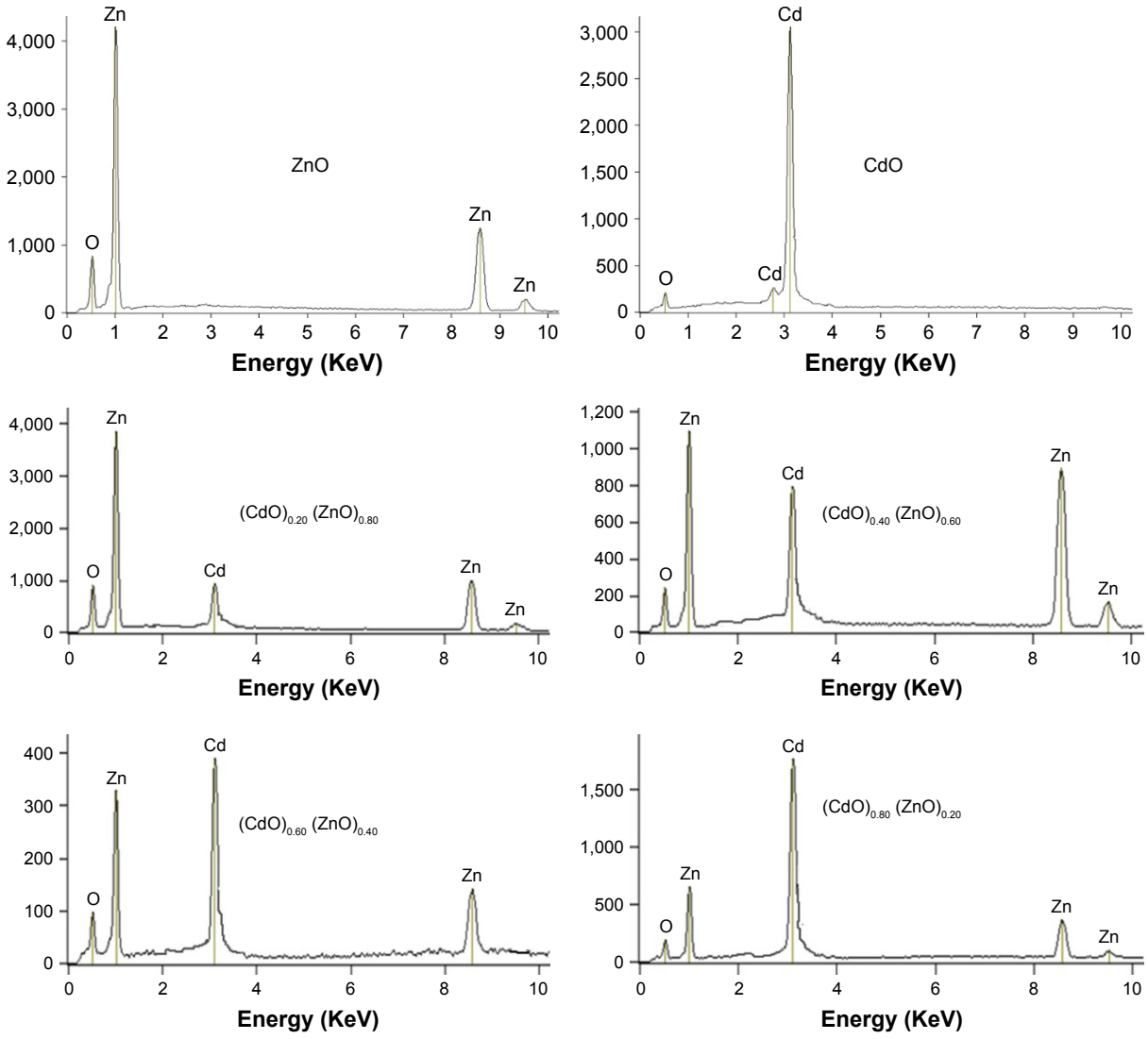

Figure 4 EDX spectrum of the $(CdO)_x$ $(ZnO)_{1-x}$ nanoparticles calcined at 600°C.
Abbreviations: EDX, energy-dispersive X-ray; ZnO, zinc oxide; CdO, cadmium oxide.

Table 1 EDX spectra showing the atomic percentages of Zn, Cd, and oxygen species in four positions

Element spectrum	Experimental results Cd:O	Zn:O	Theoretical results Cd:O	Zn:O
ZnO	–	50.13:49.87	–	50.00:50.00
CdO	50.15:49.85	–	50.00:50.00	–
$(CdO)_{0.20}$ $(ZnO)_{0.80}$	9.84:9.75	40.41:40.00	10.00:10.00	40.00:40.00
$(CdO)_{0.40}$ $(ZnO)_{0.60}$	20.43:19.27	30.05:30.25	20.00:20.00	30.00:30.00
$(CdO)_{0.60}$ $(ZnO)_{0.40}$	30.67:30.03	20.10:19.20	30.00:30.00	20.00:20.00
$(CdO)_{0.80}$ $(ZnO)_{0.20}$	39.87:40.00	10.00:10.13	40.00:40.00	10.00:10.00

Abbreviations: EDX, energy-dispersive X-ray; ZnO, zinc oxide; CdO, cadmium oxide.

morphology of the NPs generated. As discussed in the preceding section, increasing x value is associated with a significant increase in particle size. This particle size increase is due to the conglomeration of many adjacent particles as a consequence of surface melting at higher x values and calcination temperatures.[83–86] All results showed that the binary $(CdO)_x$ $(ZnO)_{1-x}$ NPs were spherical[87] and homogeneous and not subject to crystal entanglement as demonstrated by TEM scans of the synthesized binary $(CdO)_x$ $(ZnO)_{1-x}$ NPs. This standard procedure has demonstrated its efficiency in generating a variety of binary oxide NPs, where a demonstrable PVP presence is shown to influence NP size as part of an agglomeration–suppression mechanism. Table 2 compares XRD and TEM results, demonstrating correlation between particle diameters of 16 and 34 nm and calcining at 600°C. PVP is demonstrated to function as a particle stabilizer, facilitating nucleation and development of the NP and promoting consistency. It is therefore employed to restrict NP size and prevent NP agglomeration.[75–78,88]

FTIR analysis

Figure 6 depicts the FTIR spectrum obtained at 280–4,000 cm^{-1} for the binary oxide NPs produced by the thermal treatment method outlined above. The double absorption peaks are

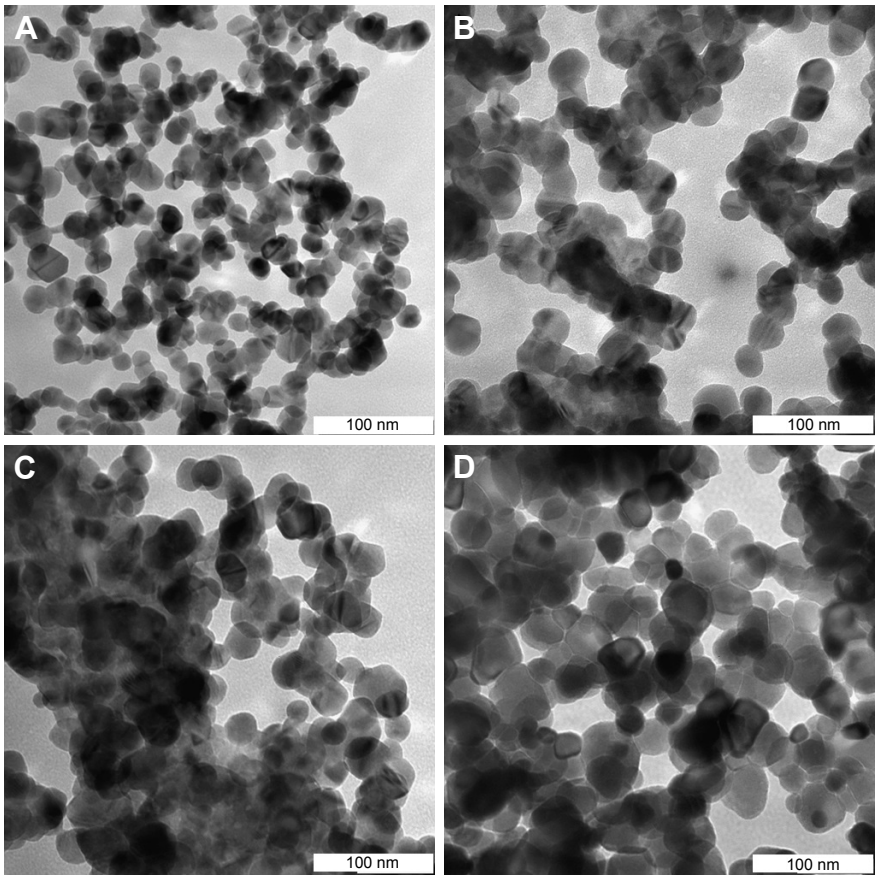

Figure 5 TEM images of (**A**) $(CdO)_{0.20}$ $(ZnO)_{0.80}$, (**B**) $(CdO)_{0.40}$ $(ZnO)_{0.60}$, (**C**) $(CdO)_{0.60}$ $(ZnO)_{0.40}$, and (**D**) $(CdO)_{0.80}$ $(ZnO)_{0.20}$ nanoparticles calcined at 600°C.
Abbreviations: TEM, transmission electron microscopy; CdO, cadmium oxide; ZnO, zinc oxide.

Table 2 XRD and TEM results for binary $(CdO)_x$ $(ZnO)_{1-x}$ nanoparticles at various x

Sample	Crystallite size (nm)	Particle size (nm)
$(CdO)_{1.00}$ $(ZnO)_{0.00}$	30±0.43	32
$(CdO)_{0.00}$ $(ZnO)_{1.00}$	31±0.36	33
$(CdO)_{0.20}$ $(ZnO)_{0.80}$	14±0.53	16
$(CdO)_{0.40}$ $(ZnO)_{0.60}$	17±0.48	18
$(CdO)_{0.60}$ $(ZnO)_{0.40}$	23±0.71	25
$(CdO)_{0.80}$ $(ZnO)_{0.20}$	32±0.64	34

Abbreviations: XRD, X-ray diffraction; TEM, transmission electron microscopy; CdO, cadmium oxide; ZnO, zinc oxide.

thought to be due to the generation of exceptionally pure binary oxide NPs, also indicated by a shift in the wave number for the $(CdO)_x$ $(ZnO)_{1-x}$ NPs spectra associated with increasing x values. This x effect is corroborated by the crystallinity enhancement of the $(CdO)_x$ $(ZnO)_{1-x}$ NPs generated. Therefore, Figure 6 demonstrates the *x*-related increment results in characteristic sharper peaks for the binary oxide, indicating that these increases in x value are associated with a more pronounced crystalline nature of the generated binary oxide.

XPS analysis

XPS analysis was employed to determine phase compositions and chemical state of Cd, Zn, and O elements. Figure 7A depicts the XPS survey spectra of binary oxide NPs, corroborating the presence of Zn, Cd, O, and C elements. Figure 7B–D depict the high-resolution XPS spectra for Cd 3d and Zn 2p. The XPS spectrum for Cd relates to respective

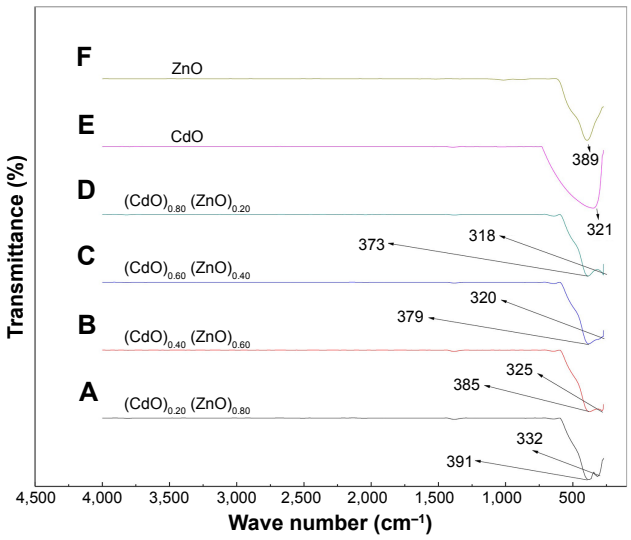

Figure 6 FTIR spectra of $(CdO)_x$ $(ZnO)_{1-x}$ nanoparticles in the range 280–4,500 at (**A**) $(CdO)_{0.20}$ $(ZnO)_{0.80}$, (**B**) $(CdO)_{0.40}$ $(ZnO)_{0.60}$, (**C**) $(CdO)_{0.60}$ $(ZnO)_{0.40}$, (**D**) $(CdO)_{0.80}$ $(ZnO)_{0.200}$, (**E**) $(CdO)_{1.00}$ $(ZnO)_{0.00}$, and (**F**) $(CdO)_{0.00}$ $(ZnO)_{1.00}$ nanoparticles calcined at 600°C.

Abbreviations: FTIR, Fourier transform infrared; CdO, cadmium oxide; ZnO, zinc oxide.

binding energies of 404.9 eV and 411.7 eV for Cd $3d_{5/2}$ and Cd $3d_{3/2}$ peaks as depicted in Figure 7B; similar results have been reported previously.[89,90] Figure 7C shows that the Zn $2p_{3/2}$ state at a binding energy of 1,021.1 eV corroborates the 2+ oxidation state of zinc.[91,92] Figure 7D depicts the deconvoluted O 1s spectrum highlighting the presence of two types of oxygen with binding energies at 529.7 eV and 531.1 eV; these correlate with ZnO and CdO, respectively.[93] These results indicate that each element within the binary NP comprises pure oxidation states with no impurities present.

Band gap analysis

The Kubelka–Munk function was utilized by plotting the square of the Kubelka–Munk function $(F(R_\infty)h\nu)^2$ versus energy and extrapolating the linear part of the curve to F $(R)^2$=0. This was employed to determine NP energy band gaps from diffuse reflectance spectra for samples calcined at temperature 600°C, as depicted in Figure 8A–F, which indicates that the band gap energy for binary oxide NPs has been produced. The energy band gaps values are observed to decrease with increasing x value. This increased x value is considered to be due to a quantum size effect. Furthermore, the reduction occurring over the band gap may be caused by the transitions between the partially suitable valance and conduction bands of the d-shell electrons of Zn^{2+} ions.[94] Therefore, exclusion of the particle size effect on the band gap presented a challenge. As a consequence of the particle size reduction, an alteration in the band structure and material properties is achievable. Conversely, NP size is increased with the band gap reduction. Therefore, at higher energy regimes, the conduction bands of s-electrons and p-electrons are separated from each other, meaning that an overlap occurrence is feasible at conditions involving smaller sized particles. At a Fermi level distance, which is extremely remote from the particle center, the nuclear potential for the conduction of electrons is very low and therefore any transition with permitted quantum numbers will possess an absorption energy equal to the conduction band energy.[95] For comparison, the band gap values were decreased with increasing x values, as depicted in Table 3. It is considered that the increase in x value may result in an increase of defected states leading to an absorption coefficient increment. Photon absorption generates electron-hole pairs. In turn, the field generated by such pairs may be able to alter the electronic structure and optical nanomaterial characteristics.

PL analysis

The PL spectra of binary oxide NPs synthesized in PVP and different concentration of precursors were recorded

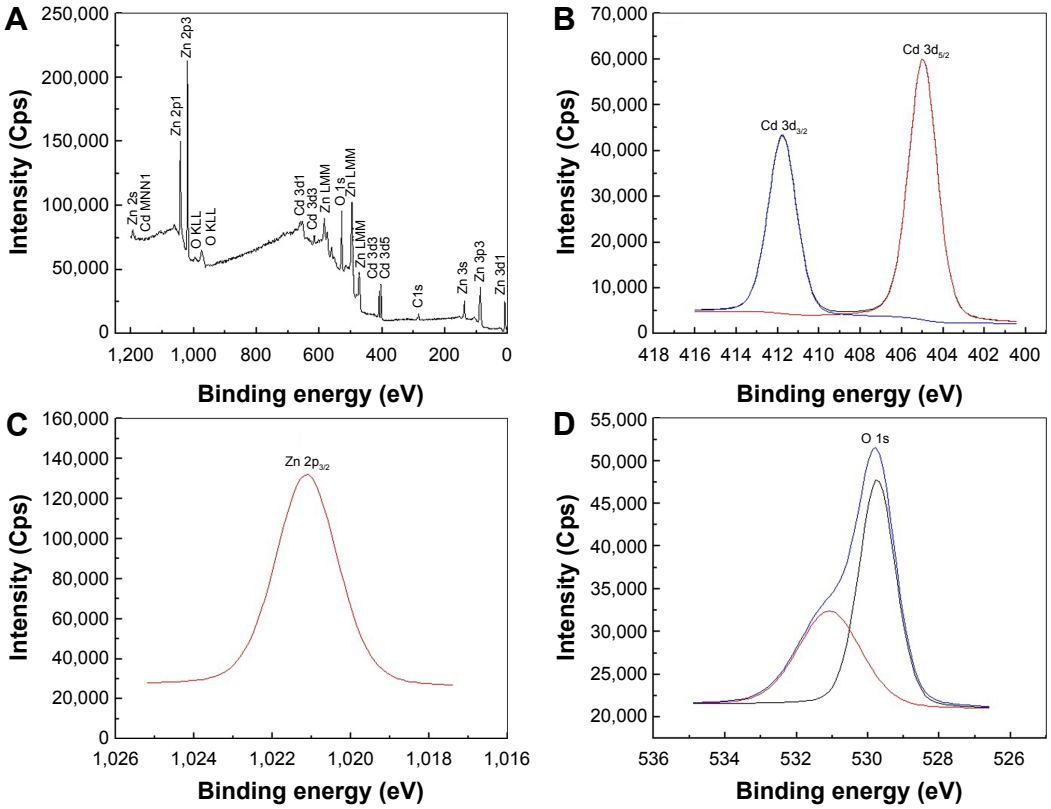

Figure 7 The XPS spectra of binary oxide nanoparticle (**A**) survey, (**B**) cadmium, (**C**) zinc, and (**D**) oxygen.
Abbreviation: XPS, X-ray photoelectron spectroscopy.

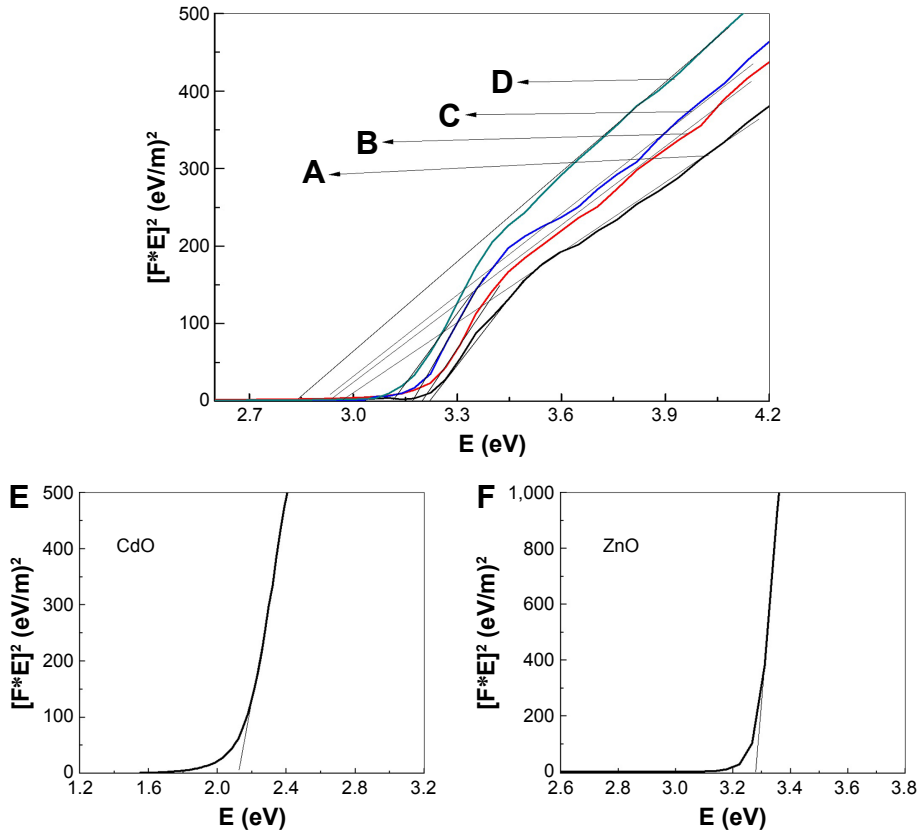

Figure 8 The energy band gap of (**A**) $(CdO)_{0.20}$ $(ZnO)_{0.80}$, (**B**) $(CdO)_{0.40}$ $(ZnO)_{0.60}$, (**C**) $(CdO)_{0.60}$ $(ZnO)_{0.40}$, (**D**) $(CdO)_{0.80}$ $(ZnO)_{0.200}$, (**E**) $(CdO)_{1.00}$ $(ZnO)_{0.00}$, and (**F**) $(CdO)_{0.00}$ $(ZnO)_{1.00}$ nanoparticles at calcination temperature of 600°C.
Abbreviations: CdO, cadmium oxide; ZnO, zinc oxide.

Table 3 Energy band gap of product at different concentrations of x

Band gap energy (eV) / $(CdO)_x$ $(ZnO)_{1-x}$ Nanoparticles	CdO Eg (eV)	ZnO Eg (eV)
x=0.00	–	3.24±0.03
x=0.20	2.92±0.07	3.22±0.05
x=0.40	2.88±0.04	3.19±0.10
x=0.60	2.84±0.08	3.15±0.02
x=0.80	2.82±0.04	3.11±0.09
x=1.00	2.12±0.10	–

Abbreviations: CdO, cadmium oxide; ZnO, zinc oxide.

at room temperature under excitation of 425 nm. Figure 9 illustrates that PL spectra associated with the binary oxide NPs prepared in PVP exhibits a broad emission scattering over a range of ~500–575 nm as a consequence of both the compounded effect and the energy states in the valence and conduction bands. These broad peaks comprise two less distinctive sub-bands at ~525 and 565 nm.[96] The first of these is thought to be due to the recombination of electron-hole pairs in oxygen and metal vacancies. The second peak (green-yellow emissions centered at 570 nm) is distinctly apparent in PL spectra of binary oxide NPs transitioning between valence and conduction bands. The peak in the wavelength range 600 nm is correlated with the deep energy levels' CdO emission, caused by the intrinsic anomalies of CdO NPs.[96,97] The PL intensities exhibit an intensification with increasing x value and attain their maximum at x=1.00 mmol, which also correlates with the maximum crystallinity attained. Comparing various precursor concentrations where increases in x values produced increases in intensity, it was observed that the peak with greatest intensity versus the weak spectral bands generated for x values below 0.80 demonstrated that x values are significant in promoting a product morphology with minimal structural and surface anomalies.

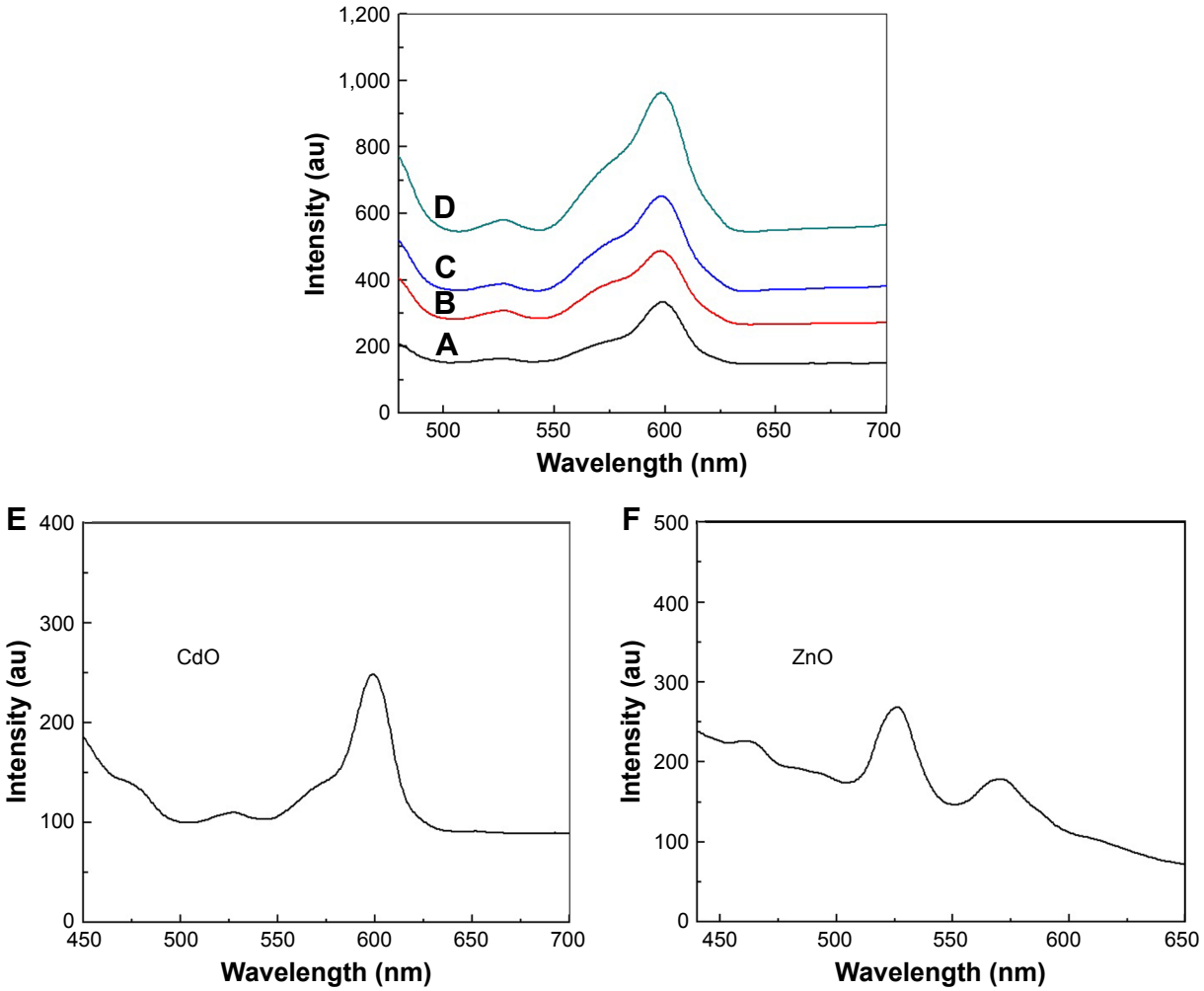

Figure 9 PL of (**A**) $(CdO)_{0.20}$ $(ZnO)_{0.80}$, (**B**) $(CdO)_{0.40}$ $(ZnO)_{0.60}$, (**C**) $(CdO)_{0.60}$ $(ZnO)_{0.40}$, (**D**) $(CdO)_{0.80}$ $(ZnO)_{0.200}$, (**E**) $(CdO)_{1.00}$ $(ZnO)_{0.00}$, and (**F**) $(CdO)_{0.00}$ $(ZnO)_{1.00}$ nanoparticles at calcination temperature of 600°C.
Abbreviations: PL, photoluminescence; CdO, cadmium oxide; ZnO, zinc oxide.

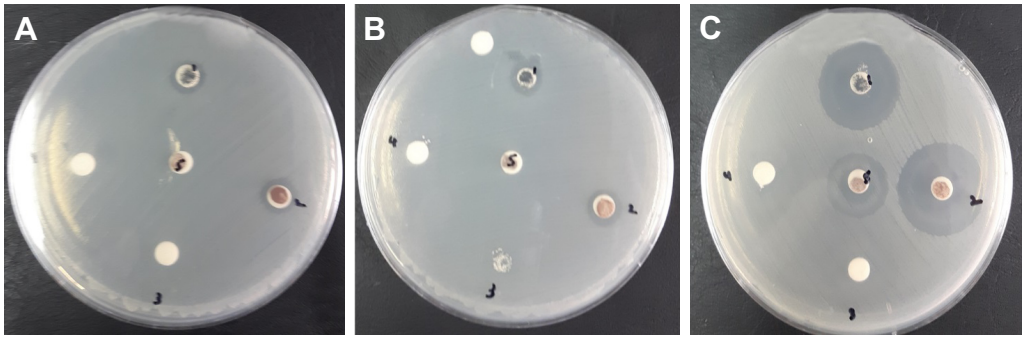

Figure 10 Inhibition zone test for (**A**) *Escherichia coli* ATCC 25922 Gram (–ve), (**B**) *Salmonella choleraesuis* ATCC 10708 Gram (–ve), and (**C**) *Bacillus subtilis* UPMC 1175 Gram (+ve).

Antibacterial activity

Figure 10 illustrates the antibacterial activity of the prepared materials ZnO bulk, ZnO NPs, binary oxide NPs, CdO bulk, and CdO NPs against *E. coli* ATCC 25922 Gram, *S. choleraesuis* ATCC 10708, and *B. subtilis* UPMC 1175 Gram (+ve). In this figure, inhibition zone diameters values used with agar plate are measured in millimeters. Results provided in Figure 11 and Table 4 are of average values. With every treated sample, three times of repeated tests were implemented and related results are provided in Table 4. Zinc oxide suspensions (4, 5) showed less antibacterial activity, while the CdO and binary NPs (1, 2, and 5) suspensions for all tested bacteria showed high antibacterial activity. These antibacterial activities for CdO and binary NPs are due to several proposed methods and mechanisms. In one of these methods, a reverse effect with the antibacterial activity increment in terms of CdO NPs size has been found. Another mechanism is that the Cd^{2+} ion release has a meaningful impact on the antibacterial activity.[98] Thus, CdO and binary NPs showed significant antibacterial activity. That has effectively showed a fatal effect versus investigated bacteria as per the *E. coli* E266 N *B. subtilis* B29 N *S. choleraesuis ATCC 10708* sequence. The CdO-ZnO NPs antibacterial efficiency has continued to relief peroxides into the used medium despite the lifeless bacteria surface has been totally shielded by binary CdO/ZnO NPs. That has shown high bactericidal ability.[99] CdO–ZnO NPs have attracted research studies to be addressed in the field of cell inhibition more than regular antibiotics have. Therefore, NP characterization for biomedical applications is desirable in the so near future.

Table 5 shows the comparison in the inhibition zone (mm) for the tested bacteria between the previously reported studies and the product obtained from this method. It is clear that this product showed an enhanced inhibition zone, which reflects a noticeably antibacterial activity. This product has the advantages of being cost-effective, ease of preparation, and higher stability.

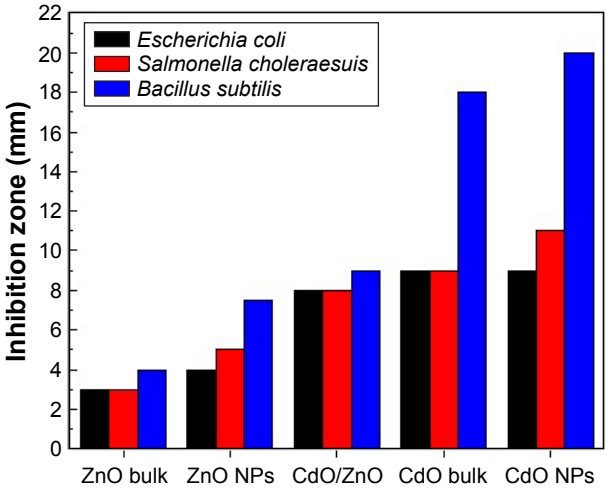

Figure 11 Average inhibition zone graph for ZnO bulk, ZnO NPs, ZnO/CdO NPs, CdO bulk, and CdO NPs against *Escherichia coli* ATCC 25922 Gram, *Salmonella choleraesuis* ATCC 10708, and *Bacillus subtilis* UPMC 1175 Gram (+ve).
Abbreviations: ZnO, zinc oxide; NP, nanoparticle; CdO, cadmium oxide.

Table 4 Average inhibition zone for ZnO bulk, ZnO NPs, ZnO/CdO NPs, CdO bulk, and CdO NPs against *Escherichia coli* ATCC 25922 Gram, *Salmonella choleraesuis* ATCC 10708, and *Bacillus subtilis* UPMC 1175 Gram (+ve)

Sample (s)	Target microbes		
	Escherichia coli ATCC 25922 Gram (–ve)	*Salmonella choleraesuis* ATCC 10708 Gram (–ve)	*Bacillus subtilis* UPMC 1175 Gram (+ve)
	Inhibition zone (mm)		
CdO bulk	9±0.4	9±1.0	18±1.6
CdO NPs	10±0.5	12±0.5	21±1.5
ZnO bulk	3±0.1	3±0.2	6.5±0.5
ZnO NPs	4±0.3	5±0.5	7.5±0.4
CdO/ZnO NPs	8±0.5	8±0.7	9±0.6

Abbreviations: ZnO, zinc oxide; NP, nanoparticle; CdO, cadmium oxide.

Table 5 Zone of inhibition presented by previously reported against *Salmonella choleraesuis, Escherichia coli* ATCC 25922 Gram (–ve), and *Bacillus subtilis*

Target microbes	Material	Inhibition zone (mm)	Concentration mg/mL	References
Salmonella choleraesuis	CdO	11 and 10	10	Xavier et al,[100] Salehi et al[101]
	ZnO	4	10	Khan et al[102]
	CdO-ZnO	–	–	Xavier et al,[100] Salehi et al,[101] Khan et al[102]
	CdO	12	10	This work
	ZnO	5	10	This work
	CdO-ZnO	8	10	This work
Escherichia coli	CdO	–	–	–
	ZnO	5	25	Khan et al[102]
	CdO-ZnO			
	CdO	10	10	This work
	ZnO	5	10	This work
	CdO-ZnO	8	10	This work
Bacillus subtilis	CdO NPs	–	–	Xavier et al,[100] Salehi et al,[101] Khan et al[102]
	ZnO NPs	–	–	Xavier et al,[100] Salehi et al,[101] Khan et al[102]
	CdO-ZnO NPs	–	–	Xavier et al,[100] Salehi et al,[101] Khan et al[102]
	CdO NPs	21±1.5	10	This work
	ZnO	7.5±0.4	10	This work
	CdO-ZnO	9±0.6	10	This work

Abbreviations: CdO, cadmium oxide; ZnO, zinc oxide; NP, nanoparticle.

Conclusion

This paper has shown that binary $(CdO)_x (ZnO)_{1-x}$ NPs were successfully prepared through thermal treatment method. Nanocrystalline binary $(CdO)_x (ZnO)_{1-x}$ were produced and characterized by face-centered cubic and hexagonal structures, respectively, at all x values, as investigated by the XRD samples analysis. The NP size was shown to be increased with an increase in x value; sizes varied from 14 nm at x=0.20 to 32 nm at x=0.80. SEM image shows a porous and grain shape, and the presence of Zn, Cd, and O atoms has been proved by EDAX analysis corresponding to those in the initial mixture. The FTIR spectrum represents the characteristic vibrational modes of Zn-O and Cd-O. The optical band gap is observed to decrease with increasing x value as demonstrated by UV–vis absorption spectrum. The luminescence spectrum shows that the intensity of PL increased with an increase in particle size. These materials have revealed that they could be used to absorb particular wavelengths of solar energy and solar cell applications.

The biological activities of the fabricated binary oxide NPs showed meaningful antibacterial activity against four pathogenic organisms. This study has indicated that the inhibition zone of 18 mm has good antibacterial activity toward the Gram-positive *B. subtilis* UPMC 1175. Experiments have demonstrated that our method outperforms the other competitive methods and can be used with a variety of biomedical and nanotechnology applications.

Acknowledgment

The authors would like to thank the Faculty of Science, Universiti Putra Malaysia for providing a suitable environment to conduct this research.

Disclosure

The authors report no conflicts of interest in this work.

References

1. Finardi U. Nanosciences and nanotechnologies: evolution trajectories and disruptive features. *Nanotechnology: Concepts, Methodologies, Tools, and Applications*. IGI Global; 2014:1–20.
2. Sekhon BS. Nanotechnology in agri-food production: an overview. *Nanotechnol Sci Appl*. 2014;7:31–53.
3. Tian J, Xu J, Zhu F, Lu T, Su C, Ouyang G. Application of nanomaterials in sample preparation. *J Chromatogr A*. 2013;1300:2–16.
4. Tang HQ, Xu M, Rong Q, Jin RW, Liu QJ, Li YL. The effect of ZnO nanoparticles on liver function in rats. *Int J Nanomed*. 2016;11:4275–4285.
5. Chan WW, Chhowalla M, Glotzer S, et al. Nanoscience and nanotechnology impacting diverse fields of science, engineering, and medicine. *ACS Nano*. 2016;10(12):10615–10617.
6. Ge Y, Li S, Wang S, Moore R. *Nanomedicine: Principles and Perspectives*. Springer-Verlag New York Inc. USA; 2014.
7. Sen P, Hegde MS, Rao CNR. Surface oxidation of cadmium, indium, tin and antimony by photoelectron and Auger spectroscopy. *Appl Surf Sci*. 1982;10(1):63–74.
8. Blum JL, Xiong JQ, Hoffman C, Zelikoff JT. Cadmium associated with inhaled cadmium oxide nanoparticles impacts fetal and neonatal development and growth. *Toxicol Sci*. 2012;126(2):478–486.
9. Zhai T, Fang X, Liao M, et al. A comprehensive review of one-dimensional metal-oxide nanostructure photodetectors. *Sensors (Basel)*. 2009;9(8):6504–6529.
10. Gupta RK, Ghosh K, Patel R, Mishra SR, Kahol PK. Structural, optical and electrical properties of In doped CdO thin films for optoelectronic applications. *Mater Lett*. 2008;62(19):3373–3375.
11. Mane RS, Pathan HM, Lokhande CD, Han SH. An effective use of nanocrystalline CdO thin films in dye-sensitized solar cells. *Sol Energy*. 2006;80(2):185–190.
12. Shukla M, Kumari S, Shukla S, Shukla RK. Potent antibacterial activity of nano CdO synthesized via microemulsion scheme. *J Mater Environ Sci*. 2012;3(4):678–685.
13. Kumar S, Ojha AK. Synthesis, characterizations and antimicrobial activities of well dispersed ultra-long CdO nanowires. *AIP Adv*. 2013;3(5):052109.
14. Yakuphanoglu F, Caglar M, Caglar Y, Ilican S. Electrical characterization of nanocluster n-CdO/p-Si heterojunction diode. *J Alloys Compd*. 2010;506(1):188–193.
15. Chandiramouli R, Jeyaprakash BG. Review of CdO thin films. *Solid State Sci*. 2013;16:102–110.
16. Srinivasaraghavan R, Chandiramouli R, Jeyaprakash BG, Seshadri S. Quantum chemical studies on CdO nanoclusters stability. *Spectrochim Acta A Mol Biomol Spectrosc*. 2013;102:242–249.

17. Fan DH. Catalyst-free growth and crystal structures of CdO nanowires and nanotubes. *J Cryst Growth*. 2009;311(8):2300–2304.
18. Peng XS, Wang XF, Wang YW, Wang CZ, Meng GW, Zhang LD. Novel method synthesis of CdO nanowires. *J Phys D: Appl Phys*. 2002; 35(20):L101.
19. Dhawale DS, More AM, Latthe SS, Rajpure KY, Lokhande CD. Room temperature synthesis and characterization of CdO nanowires by chemical bath deposition (CBD) method. *Appl Surf Sci*. 2008;254(11):3269–3273.
20. Dong W, Zhu C. Optical properties of surface-modified CdO nanoparticles. *Opt Mater*. 2003;22(3):227–233.
21. Al-Hada NM, Saion EB, Shaari AH, et al. A facile thermal-treatment route to synthesize the semiconductor CdO nanoparticles and effect of calcination. *Mater Sci Semicond Process*. 2014;26:460–466.
22. Ghoshal T, Kar S, De SK. Morphology controlled solvothermal synthesis of Cd(OH)2 and CdO micro/nanocrystals on Cd foil. *Appl Surf Sci*. 2009;255(18):8091–8097.
23. Henríquez R, Grez P, Muñoz E, Dalchiele EA, Marotti RE, Gómez H. Template-free non-aqueous electrochemical growth of CdO nanorods. *Thin Solid Films*. 2011;520(1):41–46.
24. Fu X, Liu J, Han T, Zhang X, Meng F, Liu J. A three-dimensional hierarchical CdO nanostructure: preparation and its improved gas-diffusing performance in gas sensor. *Sens Actuators B: Chem*. 2013;184: 260–267.
25. Zhang YQ, Li Z, Ling T, Kulinich SA, Du XW. Superior gas-sensing performance of amorphous CdO nanoflake arrays prepared at room temperature. *J Mater Chem A*. 2016;4(22):8700–8706.
26. Rajput JK, Pathak TK, Kumar V, Purohit LP. Influence of sol concentration on CdO nanostructure with gas sensing application. *Appl Surf Sci*. 2017;409:8–16.
27. Sreekanth TVM, Pandurangan M, Dillip GR, Kim DH, Lee YR. Toxicity and efficacy of CdO nanostructures on the MDCK and Caki-2 cells. *J Photochem Photobiol B: Biol*. 2016;164:174–181.
28. Chen YL, Hu ZA, Chang YQ, et al. Zinc oxide/reduced graphene oxide composites and electrochemical capacitance enhanced by homogeneous incorporation of reduced graphene oxide sheets in zinc oxide matrix. *The J Phys Chem C*. 2011;115(5):2563–2571.
29. Kołodziejczak-Radzimska A, Jesionowski T. Zinc oxide – from synthesis to application: a review. *Materials*. 2014;7(4):2833–2881.
30. Wang ZL. Zinc oxide nanostructures: growth, properties and applications. *J Phys: Condens Matter*. 2004;16(25):R829–R858.
31. Ali SS, Morsy R, El-Zawawy NA, Fareed MF, Bedaiwy MY. Synthesized zinc peroxide nanoparticles (ZnO2-NPs): a novel antimicrobial, anti-elastase, anti-keratinase, and anti-inflammatory approach toward polymicrobial burn wounds. *Int J Nanomed*. 2017;12:6059–6073.
32. Brayner R, Ferrari-Iliou R, Brivois N, Djediat S, Benedetti MF, Fiévet F. Toxicological impact studies based on Escherichia coli bacteria in ultrafine ZnO nanoparticles colloidal medium. *Nano Lett*. 2006; 6(4):866–870.
33. Jones N, Ray B, Ranjit KT, Manna AC. Antibacterial activity of ZnO nanoparticle suspensions on a broad spectrum of microorganisms. *FEMS Microbiol Lett*. 2008;279(1):71–76.
34. Salah N, Habib SS, Khan ZH, et al. High-energy ball milling technique for ZnO nanoparticles as antibacterial material. *Int J Nanomed*. 2011;6:863–869.
35. Hau SK, Yip HL, Baek NS, Zou J, O'Malley K, Jen AKY. Air-stable inverted flexible polymer solar cells using zinc oxide nanoparticles as an electron selective layer. *Appl Phys Lett*. 2008;92(25):225.
36. Facchetti A, Marks T. *Transparent Electronics: from Synthesis to Applications*. Chichester, U.K: John Wiley & Sons; 2010.
37. Ellmer K, Klein A, Rech B. *Transparent Conductive Zinc Oxide: Basics and Applications in Thin Film Solar Cells*. Vol 104: Springer-Verlag Berlin Heidelberg Germany; 2007.
38. Becheri A, Dürr M, Nostro PL, Baglioni P. Synthesis and characterization of zinc oxide nanoparticles: application to textiles as UV-absorbers. *J Nanopart Res*. 2008;10(4):679–689.
39. Huang MH, Wu Y, Feick H, Tran N, Weber E, Yang P. Catalytic growth of zinc oxide nanowires by vapor transport. *Adv Mater*. 2001;13(2): 113–116.
40. Zhang Y, Nayak TR, Hong H, Cai W. Biomedical applications of zinc oxide nanomaterials. *Curr Mol Med*. 2013;13(10):1633–1645.
41. Hsu JW, Tian ZR, Simmons NC, Matzke CM, Voigt JA, Liu J. Directed spatial organization of zinc oxide nanorods. *Nano Lett*. 2005; 5(1):83–86.
42. Foo KL, Hashim U, Muhammad K, Voon CH. Sol–gel synthesized zinc oxide nanorods and their structural and optical investigation for optoelectronic application. *Nanoscale Res Lett*. 2014;9(1):429.
43. Katwal G, Paulose M, Rusakova IA, Martinez JE, Varghese OK. Rapid growth of zinc oxide nanotube–nanowire hybrid architectures and their use in breast cancer-related volatile organics detection. *Nano Lett*. 2016;16(5):3014–3021.
44. Kim H, Sigmund W. Zinc oxide nanowires on carbon nanotubes. *Appl Phys Lett*. 2002;81(11):2085–2087.
45. Kachynski AV, Kuzmin AN, Nyk M, Roy I, Prasad PN. Zinc oxide nanocrystals for non-resonant nonlinear optical microscopy in biology and medicine. *J Phys Chem C Nanomater Interfaces*. 2008;112(29): 10721–10724.
46. Bai S, Quan L, Tang P, et al. Controllable synthesis and gas-sensing properties of zinc oxide nanocrystals with exposed different percentage of facets. *IEEE Sens J*. 2016;16(4):866–872.
47. Lai L, Zhao C, Su M, et al. In vivo target bio-imaging of Alzheimer's disease by fluorescent zinc oxide nanoclusters. *Biomater Sci*. 2016; 4(7):1085–1091.
48. Viswanathamurthi P, Bhattarai N, Kim HY, Lee DR. The photoluminescence properties of zinc oxide nanofibres prepared by electrospinning. *Nanotechnology*. 2003;15(3):320.
49. Kavosh M, Moallemian H, Molaei H, Mehranniya H, Salami M, Dehdashti ME. Study of optical and structural properties of zinc oxide nanofibers by using Zn(ac) 2/PVA precursors. *Synth React Inorg Met-Org Nano-Metal Chem*. 2016;46(2):225–229.
50. Kumar R, Al-Dossary O, Kumar G, Umar A. Zinc oxide nanostructures for NO2 gas–sensor applications: a review. *Nano-Micro Lett*. 2015; 7(2):97–120.
51. Cauda V, Pugliese D, Garino N, et al. Multi-functional energy conversion and storage electrodes using flower-like zinc oxide nanostructures. *Energy*. 2014;65:639–646.
52. Kumar SS, Venkateswarlu P, Rao VR, Rao GN. Synthesis, characterization and optical properties of zinc oxide nanoparticles. *Int Nano Lett*. 2013;3(1):30.
53. Quirino MR, Oliveira MJC, Keyson D, Lucena GL, Oliveira JB, Gama L. Synthesis of zinc oxide by microwave hydrothermal method for application to transesterification of soybean oil (biodiesel). *Mater Chem Phys*. 2017;185:24–30.
54. Xiong HM, Shchukin DG, Möhwald H, Xu Y, Xia YY. Sonochemical synthesis of highly luminescent zinc oxide nanoparticles doped with magnesium(II). *Angew Chem Int Ed Engl*. 2009;48(15): 2727–2731.
55. Rayathulhan R, Sodipo BK, Aziz AA. Nucleation and growth of zinc oxide nanorods directly on metal wire by sonochemical method. *Ultrason Sonochem*. 2017;35(Pt A):270–275.
56. Atchudan R, Edison TNJI, Perumal S, Karthikeyan D, Lee YR. Facile synthesis of zinc oxide nanoparticles decorated graphene oxide composite via simple solvothermal route and their photocatalytic activity on methylene blue degradation. *J Photochem Photobiol B*. 2016; 162:500–510.
57. Gnanasangeetha D, SaralaThambavani D. One pot synthesis of zinc oxide nanoparticles via chemical and green method. *Res J Mater Sci*. 2013;2320:6055.
58. Das D, Datta AK, Kumbhakar DV, Ghosh B, Pramanik A, Gupta S. Conditional optimisation of wet chemical synthesis for pioneered ZnO nanostructures. *Nano-Structures Nano-Objects*. 2017;9:26–30.
59. Al-Hada NM, Saion EB, Shaari AH, et al. A facile thermal-treatment route to synthesize ZnO nanosheets and effect of calcination temperature. *PLoS One*. 2014;9(8):e103134.
60. Farrag AA, Balboul MR. Nano ZnO thin films synthesis by sol–gel spin coating method as a transparent layer for solar cell applications. *J Sol-Gel Sci Technol*. 2017;82(1):269–279.

61. El Ghoul J, Barthou C, El Mir L. Synthesis by sol–gel process, structural and optical properties of nanoparticles of zinc oxide doped vanadium. *Superlattices Microstruct*. 2012;51(6):942–951.
62. Zheng Z, Gan L, Li H, et al. A fully transparent and flexible ultraviolet–visible photodetector based on controlled electrospun ZnO-CdO heterojunction nanofiber arrays. *Adv Funct Mater*. 2015;25(37):5885–5894.
63. Pathak TK, Rajput JK, Kumar V, Purohit LP, Swart HC, Kroon RE. Transparent conducting ZnO-CdO mixed oxide thin films grown by the sol-gel method. *J Colloid Interface Sci*. 2017;487:378–387.
64. Choi YS, Lee CG, Cho SM. Transparent conducting ZnxCd1− xO thin films prepared by the sol-gel process. *Thin Solid Films*. 1996; 289(1–2):153–158.
65. Karthik K, Dhanuskodi S, Gobinath C, Sivaramakrishnan S. Microwave-assisted synthesis of CdO–ZnO nanocomposite and its antibacterial activity against human pathogens. *Spectrochim Acta A: Mol Biomol Spectrosc*. 2015;139:7–12.
66. Sahu N, Duchaniya RK. Synthesis of ZnO-CdO nanocomposites. *J Mater Sci Surf Eng*. 2013;1(1):11–14.
67. Saravanan R, Gracia F, Khan MM, et al. ZnO/CdO nanocomposites for textile effluent degradation and electrochemical detection. *J Mol Liq*. 2015;209:374–380.
68. Ziabari AA, Ghodsi FE. Optoelectronic studies of sol–gel derived nanostructured CdO–ZnO composite films. *J Alloys Compd*. 2011; 509(35):8748–8755.
69. Saravanan R, Shankar H, Prakash T, Narayanan V, Stephen A. ZnO/CdO composite nanorods for photocatalytic degradation of methylene blue under visible light. *Mater Chem Phys*. 2011;125(1):277–280.
70. Ghosh M, Raychaudhuri AK. Structure and optical properties of Cd-substituted ZnO (Zn1−xCdxO) nanostructures synthesized by the high-pressure solution route. *Nanotechnology*. 2007;18(11):115618.
71. Sundar SM, Mahadevan CK, Ramanathan P. On the preparation of ZnO–CdO nanocomposites. *Mater Manuf Processes*. 2007;22(3):400–403.
72. Senthil K, Tak Y, Seol M, Yong K. Synthesis and characterization of ZnO nanowire–CdO composite nanostructures. *Nanoscale Res Lett*. 2009;4(11):1329–1334.
73. Kamari HM, Al-Hada NM, Saion E, et al. Calcined solution-based PVP influence on ZnO semiconductor nanoparticle properties. *Crystals*. 2017;7(2):2.
74. Al-Hada NM, Saion E, Kamari HM, et al. Structural, morphological and optical behaviour of PVP capped binary (ZnO) 0.4 (CdO) 0.6 nanoparticles synthesised by a facile thermal route. *Mater Sci Semicond Process*. 2016;53:56–65.
75. Izu N, Uchida T, Matsubara I, Itoh T, Shin W, Nishibori M. Formation mechanism of monodispersed spherical core–shell ceria/polymer hybrid nanoparticles. *Mater Res Bull*. 2011;46(8):1168–1176.
76. Koczkur KM, Mourdikoudis S, Polavarapu L, Skrabalak SE. Polyvinylpyrrolidone (PVP) in nanoparticle synthesis. *Dalton Trans*. 2015; 44(41):17883–17905.
77. Thanh NT, Maclean N, Mahiddine S. Mechanisms of nucleation and growth of nanoparticles in solution. *Chem Rev*. 2014;114(15): 7610–7630.
78. Visaveliya N, Köhler JM. Control of shape and size of polymer nanoparticles aggregates in a single-step microcontinuous flow process: a case of flower and spherical shapes. *Langmuir*. 2014;30(41):12180–12189.
79. Saravanan R, Mansoob Khan M, Gupta VK, et al. ZnO/Ag/CdO nanocomposite for visible light-induced photocatalytic degradation of industrial textile effluents. *J Colloid Interface Sci*. 2015;452:126–133.
80. Li XF, Cao Y, Sui YR, et al. Structure and optical properties of ternary ZnCdO nanopowder synthesized by sol–gel method. *Superlattices Microstruct*. 2014;69:187–193.
81. Karami H, Aminifar A, Tavallali H, Namdar ZA. PVA-based sol–gel synthesis and characterization of CdO–ZnO nanocomposite. *J Cluster Sci*. 2010;21(1):1–9.
82. Raja S, Bhuvaneswari PV, Ramesh Babu R, Gokulakrishnan V, Ramamurthi K. Studies on the structural, morphological, electrical and optical properties of (CdO) x (ZnO)1−x thin films deposited by spray pyrolysis method. *J Mater Sci: Mater Electron*. 2016;27(8): 8111–8117.
83. Al-Hada NM, Saion EB, Shaari AH, Kamarudeen MA, Flaifel MH, Gene SA. Synthesis, structural and morphological properties of cadmium oxide nanoparticles prepared by thermal treatment method. *Adv Mater Res*. 2015;1107:291–294.
84. Baqer AA, Matori KA, Al-Hada NM, Shaari AH, Saion E, Chyi JLY. Effect of polyvinylpyrrolidone on cerium oxide nanoparticle characteristics prepared by a facile heat treatment technique. *Results Phys*. 2017;7:611–619.
85. Lee PJ, Saion E, Al-Hada NM, Soltani N. A simple up-scalable thermal treatment method for synthesis of ZnO nanoparticles. *Metals*. 2015;5(4):2383–2392.
86. Salem A, Saion E, Al-Hada NM, et al. Synthesis and characterization of CdSe nanoparticles via thermal treatment technique. *Results in Physics*. 2017;7:1556–1562.
87. Mosquera E, del Pozo I, Morel M. Structure and red shift of optical band gap in CdO–ZnO nanocomposite synthesized by the sol gel method. *J Solid State Chem*. 2013;206:265–271.
88. Al-Hada NM, Saion E, Talib ZA, Shaari AH. The impact of polyvinylpyrrolidone on properties of cadmium oxide semiconductor nanoparticles manufactured by heat treatment technique. *Polymers*. 2016;8(4):113.
89. Yousef A, Barakat NA, Al-Deyab SS, Nirmala R, Pant B, Kim HY. Encapsulation of CdO/ZnO NPs in PU electrospun nanofibers as novel strategy for effective immobilization of the photocatalysts. *Colloids Surf A: Physicochem Eng Aspects*. 2012;401:8–16.
90. King PD, Veal TD, Schleife A, et al. Valence-band electronic structure of CdO, ZnO, and MgO from x-ray photoemission spectroscopy and quasi-particle-corrected density-functional theory calculations. *Phys Rev B*. 2009;79(20):205205.
91. Anandan S, Ohashi N, Miyauchi M. ZnO-based visible-light photocatalyst: band-gap engineering and multi-electron reduction by co-catalyst. *Appl Catal B*. 2010;100(3):502–509.
92. Kumar PS, Selvakumar M, Bhagabati P, Bharathi B, Karuthapandian S, Balakumar S. CdO/ZnO nanohybrids: facile synthesis and morphologically enhanced photocatalytic performance. *RSC Adv*. 2014;4(62): 32977–32986.
93. Saravanan R, Khan MM, Gupta VK, et al. ZnO/Ag/CdO nanocomposite for visible light-induced photocatalytic degradation of industrial textile effluents. *J Colloid Interface Sci*. 2015;452:126–133.
94. Tabet-Derraz H, Benramdane N, Nacer D, Bouzidi A, Medles M. Investigations on Zn x Cd 1− x O thin films obtained by spray pyrolysis. *Sol Energy Mater Sol Cells*. 2002;73(3):249–259.
95. Caglar Y, Caglar M, Ilican S, Ates A. Morphological, optical and electrical properties of CdZnO films prepared by sol–gel method. *J Phys D: Appl Phys*. 2009;42(6):065421.
96. Zhang J, Zhao SQ, Zhang K, Zhou JQ, Cai YF. A study of photoluminescence properties and performance improvement of Cd-doped ZnO quantum dots prepared by the sol–gel method. *Nanoscale Res Lett*. 2012;7(1):405.
97. Vijayalakshmi S, Venkataraj S, Jayavel R. Characterization of cadmium doped zinc oxide (Cd: ZnO) thin films prepared by spray pyrolysis method. *J Phys D: Appl Phys*. 2008;41(24):245403.
98. Khan Z, Rehman A, Hussain SZ, Nisar MA, Zulfiqar S, Shakoori AR. Cadmium resistance and uptake by bacterium, Salmonella enterica 43C, isolated from industrial effluent. *AMB Express*. 2016;6(1):54.
99. Kohen R, Nyska A. Oxidation of biological systems: oxidative stress phenomena, antioxidants, redox reactions, and methods for their quantification. *Toxicol Pathol*. 2002;30(6):620–650.
100. Xavier AR, Ravichandran AT, Ravichandran K, Mantha S, Ravinder D. Sm doping effect on structural, morphological, luminescence and antibacterial activity of CdO nanoparticles. *J Mater Sci: Mater Electron*. 2016;27(11):11182–11187.
101. Salehi B, Mehrabian S, Ahmadi M. Investigation of antibacterial effect of Cadmium Oxide nanoparticles on Staphylococcus aureus bacteria. *J Nanobiotechnol*. 2014;12(1):26.
102. Khan MF, Hameedullah M, Ansari AH, et al. Flower-shaped ZnO nanoparticles synthesized by a novel approach at near-room temperatures with antibacterial and antifungal properties. *Int J Nanomed*. 2014;9:853–864.